

Muon number violating processes in nuclei

T.S. KOSMAS^{a,b}, J.D. VERGADOS^a, and AMAND FAESSLER^b

^a *Theoretical Physics Division, University of Ioannina, GR-45110 Ioannina, Greece*

^b *Institut für Theoretische Physik der Universität Tübingen, D-72076 Tübingen, Germany*

Abstract

The flavour violating neutrinoless muon decays in the presence of nuclei, are discussed. We focus on the theoretical aspects of $\mu^-(A, Z) \rightarrow e^-(A, Z)^$ (muon to electron conversion), one of the most prominent flavour changing reactions, emphasizing its connection with the physics beyond the standard model. This process offers the most severe limits of the lepton flavour violation. By using the nuclear transition matrix elements calculated with several methods, and the recent experimental data of the branching ratio $R_{\mu e^-}$, we determine limits for the flavour changing parameters entering the elementary sector part of $R_{\mu e^-}$. These results are discussed in view of the ongoing experiment at PSI and the designed at Brookhaven, which are expected to push down by some orders of magnitude the experimental sensitivity the next few years with the hope to see “new physics”.*

1 Introduction

In the framework of the standard model of the electroweak interactions, if one associates with each lepton generation a lepton flavour quantum number as

$$\begin{pmatrix} e^- \\ \nu_e \end{pmatrix} \rightarrow L_e, \quad \begin{pmatrix} \mu^- \\ \nu_\mu \end{pmatrix} \rightarrow L_\mu, \quad \begin{pmatrix} \tau^- \\ \nu_\tau \end{pmatrix} \rightarrow L_\tau \quad (1)$$

(for antiparticles L_e, L_μ, L_τ take values with opposite sign), the quantum numbers L_e, L_μ, L_τ are separately conserved. In addition, the total lepton number

$$L = L_e + L_\mu + L_\tau \quad (2)$$

appears also to be conserved [1]-[4]. Even though these conservation laws are uncontradicted with experiment [5, 6], the standard model is believed to be an effective low energy approximation of a more fundamental theory which is unbroken at high energies. In this spirit, many theories beyond the standard model have been developed during the last decades (grand unified models, supersymmetric theories etc.) [7]-[13]. in which the existence of flavour and lepton changing effective currents is predicted. In this way, a plethora of exotic processes, non-conserving the flavour, L_e, L_μ, L_τ , and/or lepton, L , quantum numbers, are possible. For some examples and the existing limits see Table 1 [2, 7]-[15].

In the present work we are going to discuss the category of neutrinoless exotic muon decays which take place in a muonic atom, i.e. in the case when a muon is bound in the field of a nucleus. In the context of the aforementioned extensions of the standard model this bound muon can give two yet non-observed processes; the conversion of μ_b^- into an electron [16]-[32],

$$\mu_b^- + (A, Z) \rightarrow e^- + (A, Z)^* \quad (\mu_b^- \rightarrow e^- \text{ conversion}) \quad (3)$$

which violates the lepton flavour quantum numbers L_e and L_μ , and the conversion of the muon μ_b^- into a positron [15],

$$\mu_b^- + (A, Z) \rightarrow e^+ + (A, Z - 2) \quad (\mu_b^- \rightarrow e^+ \text{ conversion}) \quad (4)$$

which violates the conservation of the total lepton L as well as the flavour L_e and L_μ quantum numbers.

The important role played by the muon as a test particle in the investigation of the electromagnetic and weak interactions with hadronic particles, has been recognized decades ago [33]. The bound in the innermost 1s atomic orbital muon μ_b^- has especially prominent role, since it gives rise to very important allowed decay modes [34, 35]. it can disappear either by decaying into an electron and two neutrinos,

$$\mu_b^- \rightarrow e^- + \bar{\nu}_e + \nu_\mu \quad (\text{muon decay in orbit}), \quad (5)$$

or by being captured by the nucleus [34, 35],

$$\mu_b^- + (A, Z) \rightarrow \nu_\mu + (A, Z - 1) \quad (\text{ordinary muon capture}) \quad (6)$$

The latter two processes conserve both lepton and flavour quantum numbers and have been well studied theoretically as well as experimentally [34, 35].

The exotic channels of Eqs. (3) and (4), are the subject of some of the most important recent experiments [5, 6] searching extensively for events involving muon number non-conservation. Up to now, these experiments have only put upper limits on the branching ratios $R_{\mu e^-}$ and $R_{\mu e^+}$, i.e. on the rates of processes (3) and (4) divided by the total rate of the ordinary muon capture reaction. For a comparison of these upper limits with those obtained from other lepton flavour violating reactions see Table 1. Obviously, the observation of any of these processes will signal “new physics” beyond the standard model and restrict the various models predicting such exotic reactions.

1.1 Basic features of the exotic muon decays in nuclei

The neutrinoless rare decays, $\mu_b^- \rightarrow e^-$ and $\mu_b^- \rightarrow e^+$ conversions in nuclei, start from the same initial state (a muon at rest in a muonic atom). Experimentally, they are both simultaneously studied. Theoretically, both of them can occur by assuming mixing of intermediate (massive) neutrinos, but (μ^-, e^-) cannot distinguish between Dirac and Majorana neutrinos while (μ^-, e^+) can proceed only if the neutrinos are Majorana particles. These processes can also be predicted by supersymmetry via the mixing of the intermediate supersymmetric particles, e.g. s-leptons (see sect. 3).

There are, however, big differences between the exotic decays (μ^-, e^-) and (μ^-, e^+) originating from the individual characteristics of their transition operators. Thus, due to its charge conserving operator, the $\mu_b^- \rightarrow e^-$ conversion can take place in one nucleon; it can proceed via the coherent mode (when the participating nucleus remains in its ground state and all nucleons participate) [11], the only measurable (μ^-, e^-) conversion channel, which is an important experimental feature.

Another experimental advantage of the (μ^-, e^-) we should mention is the fact that, a detection of only one particle is sufficient and there is no need for coincidence measurement [5]. If the electron energy is equal to $E_e \approx m_\mu c^2 - \epsilon_b$ (coherent mode) the process is free from the reaction induced background which involves, in addition to the muon decay in orbit mentioned above, the following reactions:

i) Muon decay in flight.

$$\mu^- \rightarrow \nu_\mu + \bar{\nu}_e + e^- \quad (7)$$

ii) Radiative muon capture followed by the creation of a fully asymmetric e^-, e^+ pair at zero energy, i.e.

$$\begin{aligned} \mu_b^- + (A, Z) &\rightarrow (A, Z - 1) + \nu_\mu + \gamma \\ &\quad | \rightarrow e^+ + e^- \end{aligned} \quad (8)$$

On the other hand, the muon to positron conversion (μ^-, e^+) , is more complex since it is a two-nucleon process; it is similar to but more complicated than the neutrinoless double beta decay

$$(A, Z) \rightarrow (A, Z \pm 2) + e^\mp e^\mp \quad (0\nu\beta\beta - \text{decay}) \quad (9)$$

which is a lepton and flavour number violating process extensively discussed in the present workshop (see e.g. [40]).

Because of its simplicity and important characteristics, the (μ^-, e^-) conversion is preferentially studied by many authors [7]-[14], and in the present work we will devote to it a rather extensive discussion. We pay special attention to the construction of the effective Hamiltonian in the framework of several common extensions of the standard model. This is subsequently used to calculate the relevant transition rates. Using the results of the branching ratio $R_{\mu e^-}$ and exploiting the existing experimental data we put limits on the flavour violating parameters (see sect. 6).

2 The (μ^-, e^-) conversion in Nuclei

2.1 Brief historical review

The first experimental searching for (μ^-, e^-) events has been done long ago by Steinberger and Wolfe [16] at Columbia Cyclotron using Cu as a target. This experiment put an upper limit for the branching ratio $R_{\mu e^-}$

$$R_{\mu e^-} = \frac{\Gamma(\mu^- \rightarrow e^-)}{\Gamma(\mu^- \rightarrow \text{capture})} \quad (10)$$

on the value $R_{\mu e^-} < 5 \times 10^{-4}$. Some years later Conversi *et al.* [17] in the synchrocyclotron at CERN using again Cu as target with two independent experiments found the limits $R_{\mu e^-} < 5 \times 10^{-5}$ and $R_{\mu e^-} < 5 \times 10^{-6}$. A Cu target was also used at TRIUMF by Bryman *et al.* [18] in the TPC experiment. From the data of this experiment the limit $R_{\mu e^-} < 2.6 \times 10^{-8}$ was extracted.

We should note that, the use of a Cu target in the aforementioned experiments had been influenced by the theoretical estimates of Weinberg and Feinberg [7] who found that, the $\mu_b^- \rightarrow e^-$ conversion branching ratio shows a maximum in the region of Cu (see also Ref. [25]).

Target different than Cu was first used at SIN (present PSI) by Badertscher *et al.* [19] in the SINDRUM spectrometer who used the isoscalar target S . The upper limit set on $R_{\mu e^-}$ by this experiment was $R_{\mu e^-} < 1.6 \times 10^{-8}$.

In another TPC experiment at TRIUMF (Bryman *et al.* [20]) a Ti target was used and pushed the upper limit of $R_{\mu e^-}$ at first to the value $R_{\mu e^-} < 1.6 \times 10^{-11}$ and some years later [21] to the value $R_{\mu e^-} < 4.6 \times 10^{-12}$.

The best upper limit on $R_{\mu e^-}$ set up to the present has been obtained by using Ti target at PSI [5] which yielded the value $R_{\mu e^-} < 7.0 \times 10^{-13}$. Recently, by using a heavy ^{208}Pb target in the SINDRUM II experiment the limit $R_{\mu e^-} < 4.6 \times 10^{-11}$ was determined [6]. This limit was an improvement by an order of magnitude over the previous limit $R_{\mu e^-} < 4.9 \times 10^{-10}$ obtained from preliminary results on Pb at TRIUMF (Ahmad *et al.* [21]).

Ongoing experiments at PSI as well as planned experiments at Brookhaven, discussed by Walter [5] in this conference, are expected to increase the experimental sensitivity by two to three orders of magnitude with the hope to see some events of the reaction (3) in the near future or to drastically push down the best upper limit of the branching ratio $R_{\mu e^-}$.

From a theoretical point of view, the basic background for the reaction $\mu_b^- \rightarrow e^-$ has been formulated by Weinberg and Feinberg [7] who assumed that this process is mediated by a virtual photon (photonic mechanism). Non-photonic contributions were included later on in the post-gauge-theory era [8]-[12]. Afterwards, a lot of new mechanisms which lead to the $\mu - e$ conversion have been proposed [30]. The mechanisms which involve intermediate neutrino mixing or mixing of intermediate s-fermions are extensively discussed in the next section.

From a nuclear physics point of view, it is important to know the transition matrix elements of the participating nucleus in processes (3) and (4). For the reaction (3) this was recently done for a series of nuclear isotopes [31] including ^{48}Ti and ^{208}Pb which are of current experimental interest [6, 23]. Several models, like shell model, local density approximation, quasi-particle RPA etc., have been employed (see sect. 4).

3 Effective Hamiltonian of (μ^-, e^-) in common extensions of SM

Some Feynman diagrams, which contribute to $\mu_b^- \rightarrow e^-$ conversion in the lowest order of perturbation theory (one loop level) are shown in Figs. 1 and 2. In Fig. 1 mixing of intermediate neutrinos and gauge bosons is involved and in Fig. 2 the mixing of neutralinos and s-leptons in a supersymmetric model is considered. In the context of these models we construct below the effective Hamiltonian for the (μ^-, e^-) conversion by first writing down the hadronic and leptonic currents of these diagrams as follows.

3.1 Hadronic currents at the nucleon level

Usually one starts from the weak vector and axial vector quark currents. By assuming a specific nucleon model, one transforms these hadronic currents to the nucleon level. For the diagrams shown in Figs. 1 and 2, one gets the following results.

i) Photonic diagrams (Figs. 1(a) and 2(a)): In this case the hadronic vertex is the usual electromagnetic coupling

$$J_\lambda^{(1)} = \bar{N}_p \gamma_\lambda N_p = \bar{N} \gamma_\lambda \frac{1}{2} (1 + \tau_3) N \quad (\text{photonic}) \quad (11)$$

N is the nucleon isodoublet, $N = \begin{pmatrix} N_p \\ N_n \end{pmatrix}$, with N_p, N_n the proton, neutron spinors.

ii) Non-photonic diagrams: There are many such diagrams contributing to the $\mu_b^- \rightarrow e^-$ conversion. The most obvious are: a) those mediated by Z-particle exchange (see Figs. 1(a),(b), 2(a),(b)) and b) the box diagrams involving either massive neutrinos and W-bosons, as in Fig. 1(c), or s-leptons and neutralinos, as in Fig. 2(c). The non-photonic hadronic current which includes all the above cases can be compactly written as

$$J_\lambda^{(2)} = \bar{N} \gamma_\lambda \frac{1}{2} \left[(3 + f_V \beta \tau_3) - (f_V \beta'' + f_A \beta' \tau_3) \gamma_5 \right] N \quad (\text{non-photonic}) \quad (12)$$

where the parameters β , β' , β'' , for the models assumed take the values

$$\beta = \begin{cases} 5/6, & W - \text{boson exchange} \\ 3/5, & \text{SUSY Box diagrams} \\ -3.46, & \text{SUSY Z - exchange} \end{cases} \quad (13)$$

$$\beta' = \begin{cases} \beta, & \text{for box diagrams} \\ 6.90, & Z - \text{exchange} \end{cases} \quad (14)$$

$$\beta'' = \begin{cases} 0, & \text{SUSY Z - exchange} \\ 1, & \text{all other cases} \end{cases} \quad (15)$$

The parameter β is defined as $\beta = \beta_1/\beta_0$, with β_0 (β_1) the isoscalar (isovector) couplings at the quark level and f_V , f_A represent the vector, axial vector static nucleon form factors ($f_A/f_V = 1.24$). We should note that, in general, the parameters β , β' and β'' are functions of $\sin^2\theta_W$. For example, in the case of Z-exchange we have $\beta' = 3/2\sin^2\theta_W = 6.90$ (for some other cases see Ref. [30]).

3.2 The leptonic currents

The corresponding leptonic currents in the diagrams of Figs. 1 and 2 are given from the following expressions.

i) photonic mechanism:

$$j_{(1)}^\lambda = \bar{u}(p_e) \left[(f_{M1} + \gamma_5 f_{E1}) i\sigma^{\lambda\nu} \frac{q_\nu}{m_\mu} + (f_{E0} + \gamma_5 f_{M0}) \gamma_\nu \left(g^{\lambda\nu} - \frac{q^\lambda q^\nu}{q^2} \right) \right] u(p_\mu) \quad (16)$$

ii) Non-photonic mechanism:

$$j_{(2)}^\lambda = \bar{u}(p_e) \gamma^\lambda \frac{1}{2} (f_1 + f_2 \gamma_5) u(p_\mu) \quad (17)$$

where $q = p_e - p_\mu$ is the momentum transfer with p_e , p_μ the lepton momenta. The parameters f_{E0} , f_{E1} , f_{M0} , f_{M1} , f_1 , f_2 are gauge model dependent form factors. In the models mentioned above they are interrelated as follows.

3.2.1 Models involving intermediate neutrinos and gauge bosons

For purely left-handed theories we have

$$f_{E0} = -f_{M0}, \quad f_{E1} = -f_{M1}, \quad f_1 = -f_2 \quad (18)$$

In models involving W -bosons, it, furthermore, holds

$$\frac{f_{E0}}{q^2} = -\frac{f_{E1}}{m_\mu^2} \quad (19)$$

3.2.2 Models involving intermediate neutralinos and s-leptons

In this case, the photonic and non-photonic parameters are related as

$$(4\pi\alpha)f_{M1} = -(4\pi\alpha)f_{E1} = -\frac{1}{24}f \quad (20)$$

$$(4\pi\alpha)f_{E0} = -(4\pi\alpha)f_{M0} = -\frac{1}{72}f \quad (21)$$

$$f_1 = -f_2 = \frac{1}{16}\beta_0 f, \quad \beta_0 = -\frac{2}{3}\sin^2\theta_w \quad (22)$$

$$f = \alpha^2 \frac{m_\mu^2}{\bar{m}^2} \tilde{\eta}, \quad \tilde{\eta} = \frac{(\delta m_{\tilde{U}}^2)_{12}}{\bar{m}^2} \quad (23)$$

\bar{m}^2 are the average of the square of the s-fermion masses and $\tilde{\eta}$ depends on the details of the model. For Z-exchange contribution in SUSY models (see also Ref. [30]) we have

$$f_1 = -f_2 = \xi \alpha^2 \frac{m_\mu^2}{m_Z^2} \tilde{\eta} \quad (24)$$

ξ depends on the specific model; it vanishes if one ignores the Higgsino components of the neutralinos (e.g. in the case of a pure photino); it also vanishes if the probabilities of finding the two Higgsinos in the neutralino are equal. In the model 2 of Ref. [41] it takes the value $\xi = 2.8 \times 10^{-2}$. In models in which \bar{m}^2 is larger than m_Z^2 , the Z-exchange is more favored. Due to the smallness of ξ , however, many authors consider Z' etc. [12].

3.3 The (μ^-, e^-) conversion effective Lagrangian at nucleon level

The effective Lagrangian at nucleon level, which contains contributions from all types of diagrams mentioned above, is written in the form

$$\mathcal{M} = \frac{4\pi\alpha}{q^2} j_{(1)}^\lambda J_\lambda^{(1)} + \frac{\zeta}{m_\mu^2} j_{(2)}^\lambda J_\lambda^{(2)} \quad (25)$$

$$(\text{Photonic}) \quad (\text{Non - photonic})$$

where α is the fine structure constant, and

$$\zeta = \begin{cases} \frac{G_F m_\mu^2}{\sqrt{2}}, & W - \text{boson exchange} \\ 1, & s - \text{lepton mixing} \end{cases} \quad (26)$$

3.4 Transition operators at the nuclear level

In order to obtain the transition operators at the nuclear level, where the calculations of the transition rates are done, one usually assumes that the lower components of the nucleon spinors is negligible. This assumption gives the non-relativistic limit of hadronic currents. For a nucleus (A, Z) this leads to the following $\mu_b^- \rightarrow e^-$ conversion operators

$$\Omega_0 = \tilde{g}_V \sum_{j=1}^A (3 + f_V \beta \tau_{3j}) e^{-i\mathbf{q}\cdot\mathbf{r}_j} \quad (\text{Vector}) \quad (27)$$

which is of Fermi-type, and

$$\Omega = -\tilde{g}_A \sum_{j=1}^A (f_V \beta'' + f_A \beta' \tau_{3j}) \frac{\sigma_j}{\sqrt{3}} e^{-i\mathbf{q}\cdot\mathbf{r}_j} \quad (\text{Axial Vector}) \quad (28)$$

which is of Gamow-Teller type ($f_V = 1.0$, $f_A = 1.24$). The parameters \tilde{g}_V and \tilde{g}_A take the values $\tilde{g}_V = 1/6$, $\tilde{g}_A = 0$, for the photonic case, and $\tilde{g}_V = \tilde{g}_A = 1/2$, for the non-photonic case.

In the calculations of the nuclear part of the transition rate, the following multipole expansion operators, obtained from Eqs. (27), (28), enter.

$$\hat{T}_M^{(l,0)J} = \delta_{lJ} \sqrt{4\pi} \sum_{i=1}^A (3 + f_V \beta \tau_{3i}) j_l(kr_i) Y_M^l(\hat{\mathbf{r}}_i) \quad (29)$$

$$\hat{T}_M^{(l,1)J} = \sqrt{4\pi} \sum_{i=1}^A (f_V \beta'' + f_A \beta' \tau_{3i}) j_l(kr_i) [Y^l(\hat{\mathbf{r}}_i) \times \sigma_i]_M^J \quad (30)$$

The matrix elements of these operators calculated in a given nuclear model provide the individual multipole contributions (see Refs. [29, 31, 32]). From kinematics one can show that the momentum transfer q can be approximated by

$$q \equiv q_f = m_\mu - \epsilon_b - (E_f - E_{gs}) \quad (31)$$

where ϵ_b represent the muon binding energy and $(E_f - E_{gs})$ the excitation energy of the nucleus (A,Z).

4 The (μ^- , e^-) conversion branching ratio $R_{\mu e^-}$

In studying the $\mu^- \rightarrow e^-$ conversion process, the most interesting quantities both theoretically and experimentally are (i) the branching ratio $R_{\mu e^-}$ defined in Eq. (10) and (ii) the ratio of coherent to total rate

$$\eta = \frac{\Gamma_{coh}(\mu \rightarrow e^-)}{\Gamma_{tot}(\mu \rightarrow e^-)} \quad (32)$$

In general, it is impossible to separate the nuclear structure dependence of $R_{\mu e^-}$ from the elementary particle parameters. In the coherent mode, however, this is sometimes possible (see Ref. [30]). In the models mentioned in the previous section the dominant coherent channel, can be written as

$$R_{\mu e^-} = \rho \gamma \quad (33)$$

where ρ is independent on nuclear physics. The function $\gamma(A, Z)$ contains all the nuclear information and is defined as

$$\gamma = \frac{E_e p_e}{m_\mu^2} \frac{M^2}{G^2 Z f_{GP}(A, Z)} \quad (34)$$

($G^2 \approx 6$) with f_{GP} the Goulard-Primakoff [34] function describing the total $\mu_b^- \rightarrow \nu_\mu$ rate and M^2 the nuclear transition matrix elements of the $\mu_b^- \rightarrow e^-$ conversion. Thus, the nuclear aspect of the $\mu - e$ conversion process involves the matrix elements M^2 which in general are given by

$$M^2 = f_V^2 |\langle f | \Omega_0 | i, \mu \rangle|^2 + 3f_A^2 |\langle f | \mathbf{\Omega} | i, \mu \rangle|^2 \quad (35)$$

where $|f\rangle$ the final nuclear state populated during the process.

The quantity η of Eq. (32), in the case of the approximation Eq. (33) can be written in terms of the matrix elements of Eq. (35) as

$$\eta = \frac{\Gamma_{coh}(\mu \rightarrow e^-)}{\Gamma_{tot}(\mu \rightarrow e^-)} \approx \frac{M_{coh}^2}{M_{tot}^2} \quad (36)$$

where M_{coh}^2 , M_{tot}^2 the coherent, total rate matrix elements, respectively. Such calculations of η are discussed in sect. 6.

4.1 Definitions of $\gamma(A, Z)$ and ρ in various models

i) Neutrino mixing models: For the photonic diagrams, the function γ of Eq. (34) takes the form

$$\gamma_{ph} = \frac{E_e p_e}{m_\mu^2} \frac{Z |F_Z(q^2)|^2}{G^2 f_{GP}(A, Z)} \quad (37)$$

For the photonic mechanism with left-handed currents only, the parameter ρ of Eq. (33) is given by

$$\rho = (4\pi\alpha)^2 \frac{|f_{M1} + f_{E0}|^2 + |f_{E1} + f_{M0}|^2}{(G_F m_\mu^2)^2} = \frac{9\alpha^2}{64\pi^2} \left| \frac{m_e^2}{m_W^2} \eta_\nu + \eta_N \right|^2 \quad (38)$$

For the non - photonic diagrams the function γ is given by Eq. (34) with M^2 given by

$$M^2 = \left[1 + \frac{3 - f_V \beta}{3 + f_V \beta} \frac{N}{Z} \frac{F_N(q^2)}{F_Z(q^2)} \right]^2 \gamma_{ph} \quad (39)$$

($F_Z(q^2)$, $F_N(q^2)$ are the proton, neutron nuclear form factors) and the parameter ρ associated with intermediate neutrinos is given by

$$\rho = \frac{|\beta_0 f_1|^2 + |\beta_0 f_2|^2}{2} = \frac{9}{64\pi^4} (G_F m_W^2)^2 \left| 30 \frac{m_e^2}{m_W^2} \eta_\nu + \eta_N \right|^2 \quad (40)$$

The quantities η_ν and η_N in Eqs. (38) and (40) are the flavour violating parameters associated with intermediate light (ν_j) or heavy (N_j) neutrinos. They depend on the gauge model (we have ignored the neutrino mass independent contribution arising from the non-unitarity of $U^{(1)}$) as

$$\eta_\nu = \sum_j U_{ej}^{(1)} U_{\mu j}^{(1)*} \frac{m_j^2}{m_e^2} \quad (41)$$

$$\eta_N = \sum_j U_{ej}^{(2)} U_{\mu j}^{(2)*} \frac{m_W^2}{M_j^2} \left(-2 \ln \frac{M_j^2}{m_W^2} + 3 \right) \quad (42)$$

$U_{ej}^{(i)}, U_{\mu j}^{(i)}$, with $i = 1$ for light neutrinos and $i = 2$ for heavy neutrinos, are the elements of the charged lepton current mixing matrix associated with the electron and the muon as

$$\nu_e = \sum_{j=1}^n U_{ej}^{(1)} \nu_j + \sum_{j=1}^n U_{ej}^{(2)} N_j \quad (43)$$

$$\nu_\mu = \sum_{j=1}^n U_{\mu j}^{(1)} \nu_j + \sum_{j=1}^n U_{\mu j}^{(2)} N_j \quad (44)$$

where ν_e, ν_μ are the weak neutrino eigenstates. The number n counts the generations assumed.

ii) Neutralino and s-lepton mixing models: Under some plausible assumptions and neglecting the Z-exchange, the function γ and the parameter ρ are given by

$$\gamma = \zeta \left(\frac{13}{12} + \frac{1}{2} \frac{N}{Z} \frac{F_N}{F_Z} \right)^2 \gamma_{ph} \quad (45)$$

$$\rho = \frac{1}{288} \frac{\alpha^4}{(G_F \bar{m}^2)^2} |\bar{\eta}|^2 \quad (46)$$

In the case of Z-exchange diagrams we have

$$\gamma = 0.053 \left(1 - 14.04 \frac{N}{Z} \frac{F_N}{F_Z} \right)^2 \gamma_{ph} \quad (47)$$

and the quantity ρ is now given by

$$\rho = 5.5 \times 10^{-4} \frac{\alpha^4}{(G_F \bar{m}^2)^2} |\bar{\eta}|^2 \quad (48)$$

We should note that, in the models discussed above, the only variables of the elementary particle sector which enter the function γ are the parameters $\beta = \beta_1/\beta_0$, β' and β'' . Once $\gamma(A, Z)$ is known, e.g. by nuclear model calculations, from Eq. (33) one can extract information about the interesting parameter ρ from the experimental data (see sects. 5 and 6).

5 Nuclear model calculations for the branching ratio $R_{\mu e^-}$

The main aim of the nuclear calculations of the $\mu^- \rightarrow e^-$ conversion is to study the nuclear structure dependence of its coherent, incoherent and total rates throughout the periodic table and find favorable nuclear systems to be used as targets in searching for lepton number non-conservation. Furthermore, by exploiting the nuclear part of the branching ratio in Eq. (33) we can put restrictions on the elementary sector part of $R_{\mu e^-}$, i.e. the quantity ρ , which contains the lepton flavour violating parameters (neutrino masses, mixing angles etc.) of a specific gauge model. In this way, one can check the models predicting flavour non-conservation and improve them.

5.1 Calculation of the muon-nucleus overlap integral

As we have seen in sect. 4, by neglecting the effect of nuclear recoil, the nuclear dependence of the $\mu - e$ conversion rate is, in general, included in the matrix elements of Eq. (35).

In the special case of the coherent process, i.e. ground state to ground state transitions, only the vector component of Eq. (35) contributes and one obtains

$$\langle f | \Omega_0 | i, \mu \rangle = \tilde{g}_V (3 + f_V \beta) \tilde{F}(q^2) \quad (49)$$

where $\tilde{F}(q^2)$ is the matrix element involving the ground state proton, $\rho_p(\mathbf{x})$, and neutron, $\rho_n(\mathbf{x})$, densities (normalized to Z and N respectively) as

$$\tilde{F}(q^2) = \tilde{F}_p(q^2) + \frac{3 - f_V \beta}{3 + f_V \beta} \tilde{F}_n(q^2) \quad (50)$$

with

$$\tilde{F}_{p,n}(q^2) = \int d^3x \rho_{p,n}(\mathbf{x}) e^{-i\mathbf{q}\cdot\mathbf{x}} \Phi_\mu(\mathbf{x}) \quad (51)$$

Thus, the coherent rate matrix elements can be obtained from Eq. (49) by firstly calculating $\tilde{F}(q^2)$ from Eq. (50) for a given muon wave function and given proton, neutron nuclear density distributions needed in Eq. (51).

The methods used up to now, according to how do they treat the muon-nucleus overlap integral appeared in the branching ratio, are classified in two categories: i) those using exact evaluation of the muon wave function, and ii) those using the factorization approximation for the muon wave function. In the next subsections we present a brief description of these methods.

5.1.1 Exact Evaluation of the muon wave function

For point like nuclei the muon wave function $\Phi_\mu(\mathbf{r})$ is trivially obtained by solving the Schrödinger or Dirac equations for the Coulombic nuclear potential. By taking into consideration the effects of finite nuclear size and vacuum polarization one needs to solve numerically these equations. Such calculations were done in Refs. [28, 42]. In Ref. [28] the muon wave function was obtained by solving numerically the Schrödinger equation taking into account the aforementioned effects. In Ref. [42] the Dirac and Schrödinger equations are solved using modern neural network techniques and an analytic expression for $\Phi_\mu(\mathbf{r})$ is obtained by means of optimization methods.

5.1.2 Factorization approximation for the muon wave function

A reasonable assumption for the $1s$ muon wave function of light and medium nuclei is to assume that it varies little inside such systems. In this case one can use for the matrix elements Eq. (49) the following approximation

$$\langle f | \Omega_0 | i, \mu \rangle \approx \tilde{g}_V (3 + f_V \beta) \langle \Phi_{1s} \rangle \langle f | \Omega_0 | i \rangle \quad (52)$$

where $\langle \Phi_{1s} \rangle$ is the mean value of the muon wave function given by

$$\langle \Phi_{1s} \rangle^2 = \frac{\alpha^3 m_\mu^3}{\pi} \frac{Z_{eff}^4}{Z} \quad (53)$$

α is the fine structure constant and Z_{eff} represents the effective charge which sees the μ_b^- in a muonic atom. For light nuclei μ_b^- lives outside the nucleus, $Z_{eff} \approx Z$, but for heavy and very heavy nuclei the μ_b^- resides inside the nucleus and $Z_{eff} \ll Z$.

Using this approximation, for the coherent rate many authors (see Ref. [7, 11, 25]) calculated the quantity $\tilde{F}(q)$ in eq. (50) from the equation

$$|\tilde{F}(q^2)|^2 \approx \frac{\alpha^3 m_\mu^3}{\pi} \frac{Z_{eff}^4}{Z} |ZF_Z(q^2) + \frac{3 - f_V \beta}{3 + f_V \beta} NF_N(q^2)|^2 \quad (54)$$

The nuclear form factors F_Z , F_N are either calculated by using various models, i.e. shell model [25, 43], quasi-particle RPA [29] etc., or extracted from experimental data whenever possible [44, 45].

The branching ratio $R_{\mu e^-}$ in this approximation takes the form of Eq. (33) with γ given as explained in sect. 4.

5.2 Evaluation of the partial $\mu^- \rightarrow e^-$ conversion rates

The methods used up to now, according to how do they evaluate the partial rates, i.e. the transition rate of each individual channel, are classified in two categories: 1) those doing state-by-state calculations of the partial rates 2) those employing an effective evaluation of the partial rates.

The first methods need an explicit construction of the final nuclear states in the context of a nuclear model (shell model, RPA, Fermi gas model etc.) and, therefore, they are, in general, more tedious. This difficulty is avoided in the approximations of the second category (see below).

5.2.1 State-by-state calculation of the $\mu - e$ conversion rates

With this method, by constructing explicitly the final nuclear states $|f\rangle$ in the context of a nuclear model, the branching ratio $R_{\mu e^-}$ is obtained by “summing the partial rates” for all possible excited states. By using the multipole expansion of the (μ^-, e^-) operators Eqs. (29) and (30), the total rate matrix elements M_{tot}^2 are evaluated by

$$M_{tot}^2 = \sum_s (2s+1) f_s^2 \left[\sum_{f_{exc}} \left(\frac{q_{exc}}{m_\mu} \right)^2 \sum_{l,J} |\langle f_{exc} || \hat{T}^{(l,s)J} || gs \rangle|^2 + \left(\frac{q_{gs}}{m_\mu} \right)^2 \sum_{l,J} |\langle gs || \hat{T}^{(l,s)J} || gs \rangle|^2 \right] \quad (55)$$

($s=0$ for the vector operator and $s=1$ for the axial vector one). The first term in the brackets of Eq. (55) contains the contribution coming from all the excited states $|f_{exc}\rangle$ of the final nucleus (incoherent rate) and the second term contains the contributions coming from the ground state to ground state (coherent rate).

State-by-state RPA calculations

In actual shell model calculations it is quite hard to construct the final states explicitly in medium and heavy nuclei. In such cases one can employ the RPA approximation. In the context of the quasi-particle RPA the final states entering the partial rate matrix elements are obtained by acting on the vacuum $|0\rangle$ with the phonon creation operator

$$Q^+(fJM) = \sum_{a,\tau} \left[X_a^{(f,J,\tau)} A^+(a, JM) - Y_a^{(f,J,\tau)} A(a, \overline{JM}) \right] \quad (56)$$

(angular momentum coupled representation) i.e. $|f\rangle = Q^+ |0\rangle$. The quantities X and Y in Eq. (56) are the forward and backward scattering amplitudes. The index a , runs over proton ($\tau = 1$) or neutron ($\tau = -1$) two particle configurations coupled to J.

The transition matrix element giving the partial rate $\Gamma_{i \rightarrow f}$ from an initial state 0^+ to an excited state $|f\rangle$ takes the form

$$\langle f || \hat{T}^{(l,S)J} || 0^+ \rangle = \sum_{a,\tau} W_a^J \left[X_a^{(f,J,\tau)} U_{j_2}^{(\tau)} V_{j_1}^{(\tau)} + Y_a^{(f,J,\tau)} V_{j_2}^{(\tau)} U_{j_1}^{(\tau)} \right] \quad (57)$$

The probability amplitudes V and U for the single particle states to be occupied and unoccupied, respectively, are determined from the BCS equations and the X and Y matrices are provided by solving the QRPA equations. The quantities $W_a^J \equiv W_{j_2 j_1}^J$ contain the reduced matrix elements of the operators \hat{T} of Eqs. (29) and (30) between the single particle proton or neutron states j_1 and j_2 as

$$W_{j_2 j_1}^J = \langle j_2 || \hat{T}^J || j_1 \rangle / (2J + 1) \quad (58)$$

5.2.2 Effective computation of the individual $\mu^- \rightarrow e^-$ partial rates

The contribution of each individual state in the total $\mu - e$ conversion rate is effectively taking into account in the methods: i) nuclear matter mapped into finite nuclei and ii) sum rule approach (closure approximation). For a short description of these methods we devote the next subsections.

1. Nuclear matter mapped into finite nuclei via a local density approximation

This method, uses the exact muon wave function and gives the incoherent rate in terms of the Lindhard function [28]

$$\bar{U}_{1,2}(q) = 2 \int \frac{d^3 p}{(2\pi)^3} \frac{n_1(\mathbf{p})[1 - n_2(\mathbf{q} + \mathbf{p})]}{q^0 + E_1(\mathbf{p}) - E_2(\mathbf{q} + \mathbf{p}) + i\epsilon} \quad (59)$$

where $n_1(\mathbf{q}')$ and $n_2(\mathbf{q})$ the integral (0 or 1) occupation probabilities of proton-particle proton-hole (or neutron-particle neutron-hole), respectively. In the $\mu - e$ conversion this function corresponds to ph excitations of p-p or n-n type.

This method resembles to the relativistic Fermi gas model and uses the local density approximation for the evaluation of the incoherent (μ^-, e^-) conversion rate, as

$$\begin{aligned} \Gamma_{inc}(\mu^- A \rightarrow e^- A^*) &= -2 \int d^3 x |\Phi_\mu(\mathbf{x})|^2 \int \frac{d^3 p_e}{(2\pi)^3} \Pi_i \frac{2m_i}{2E_i} \\ &\times [\bar{\Sigma}\Sigma|T|^2(\mu^- p \rightarrow e^- p) Im\bar{U}_{p,p}(p_\mu - p_e) \\ &+ \bar{\Sigma}\Sigma|T|^2(\mu^- n \rightarrow e^- n) Im\bar{U}_{n,n}(p_\mu - p_e)] \end{aligned} \quad (60)$$

T represents the transition matrix, i.e. the amplitude associated with the elementary processes $\mu^- p \rightarrow e^- p$ and $\mu^- n \rightarrow e^- n$, and m_i, E_i are the masses, energies of the particles involved in these reactions. The two terms in the brackets of Eq. (60) result because of the charge conserving character of the (μ^-, e^-) operator.

One can separate the nuclear dependence from the dependence on the elementary sector in Eq. (60) by factorizing outside the integral of eq. (60) an average value of the quantity $\bar{\Sigma}\Sigma|T|^2$. For the ratio R of the incoherent (μ^- , e^-) rate divided by the total muon capture rate, we get

$$R = \frac{\Gamma_{inc}(\mu^-, e^-)}{\Gamma(\mu^-, \nu_\mu)} = \frac{f_1^2 + f_2^2}{2} \left(\frac{\beta_0(3 + \beta)}{2} \right)^2 G(A, Z) \quad (61)$$

(the second step holds for the non-photonic case, involving the box diagrams of Fig. 1(c)). All the nuclear information is contained in the function $G(A, Z)$ defined in Ref. [28]. Notice that R differs from the branching ratio $R_{\mu e^-}$, because R does not include the coherent part of the (μ^- , e^-) process. The calculation of R in various nuclei is based upon $G(A, Z)$, since the $|T|^2$ at the elementary level is in most models independent on the nuclear parameters.

The branching ratio $R_{\mu e^-}$ in this method is obtained by adding in eq. (61) the quantity

$$R' = \frac{\Gamma_{coh}(\mu^- \rightarrow e^-)}{\Gamma(\mu^- \rightarrow \nu_\mu)} \quad (62)$$

calculated independently. To calculate R' one can use the experimental data for the nuclear form factors (electron scattering, pionic atoms data etc. [45]) and the muon capture data [35].

2. Sum rule approach

In the closure approximation, the contribution of each final state $|f\rangle$ to the total rate is also approximately taken into account. One assumes a mean excitation energy of the nucleus $\bar{E} = \langle E_f \rangle - E_{gs}$, uses completeness relation for the final states $|f\rangle$, i.e. $\sum_f |f\rangle\langle f| = 1$, and avoids the construction of each final state explicitly.

The method proceeds by defining the operator taken as a tensor product from the single-particle operators \hat{T} of Eq. (29) or (30). For a 0^+ initial (ground) state the relevant tensor product is

$$\hat{O} = \sum_{k,k'} [\hat{T}^k \times \hat{T}^{k'}]_0^0 \quad (63)$$

The corresponding total rate matrix elements are then written as

$$M_{tot}^2 = \left(\frac{|\mathbf{k}|}{m_\mu} \right)^2 [f_V^2 \langle i | \hat{O}_V | i \rangle + 3f_A^2 \langle i | \hat{O}_A | i \rangle] \quad (64)$$

where $|\mathbf{k}|$ is the average momentum transfer. The operators \hat{O}_V (vector) and \hat{O}_A (axial vector) contain both one-body and two-body pieces. Consequently, in the closure approximation one has to evaluate the matrix elements of the operators \hat{O}_V , \hat{O}_A in the ground state $|i\rangle$ described by a specific nuclear model.

The mean excitation energy \bar{E} of the nucleus, involved in the matrix elements is defined as [34]

$$\bar{E} = \frac{\sum_f (E_f - E_{gs}) q_f^2 |\langle f | \hat{T}^J | gs \rangle|^2}{\sum_f q_f^2 |\langle f | \hat{T}^J | gs \rangle|^2} \quad (65)$$

where the numerator represents the energy weighted sum rule and the denominator the non-energy weighted sum rule.

Obviously, the mean excitation energy \bar{E} should be evaluated by constructing explicitly all the possible excited states $|f\rangle$ in the context of a nuclear model. But in the closure approximation one wishes to avoid such calculations. Fortunately, \bar{E} does not strongly depend on (A, Z) and its calculation for some properly chosen representative nuclei enables the use of closure for every nucleus throughout the periodic table. In Ref. [29], the QRPA method has been used for the determination of the mean excitation energy for some nuclear isotopes including ^{48}Ti and ^{208}Pb which are of current experimental interest.

6 Results and Discussion

6.1 Nuclear structure dependence of the $\mu^- \rightarrow e^-$ conversion rates

The nuclear physics calculations done for the (μ^-, e^-) conversion mainly refer to the most interesting quantities of the process, i.e. the branching ratio $R_{\mu e^-}$ and the ratio η of Eq. (32). Several nuclear methods for the most important mechanisms leading to this process have been employed. A general feature of the results obtained for various types of diagrams is the fact that qualitatively they are very similar (see as an example Fig. 3 below). The quantitative differences are mainly related to the presence or not of neutron contributions (they exist only for non-photonic diagrams) and the different values of the parameters β, β' and β'' of Eqs. (13), (14) and (15) which are the only elementary physics parameters entering the nuclear transition matrix elements.

For the coherent rate and the total rate obtained using a sum rule approach, only the ground state of the nucleus need be constructed. The first such extensive calculations for closed (sub)shell nuclei were done with a determinantal ground state wave function (Slater determinant). These calculations provided a good description of the coherent rate [27]. The sum-rule results, however, have shown that the total rates are sensitive to the mean excitation energy required in the closure approximation. Furthermore, the local density approximation [28] gives reliable results for the coherent rate mainly due to the exact computation of the muon-nucleus overlap integral. The main advantage of this method in calculating the incoherent rate (by integrating over a continuum of excited states of a local Fermi sea), is the fact that it takes into account the contributions coming from the continuum, which are not explicitly included in RPA and shell model results.

Below we discuss the results obtained in the framework of the quasi-particle RPA and discuss their comparison with those of shell model and local density approximation. The coherent and incoherent rate are discussed separately.

6.1.1 The coherent process

As we have mentioned in sect. 5, for the coherent rate the proton, $F_Z(q^2)$, and neutron, $F_N(q^2)$, nuclear form factors are required. The results obtained by using quasiparticle RPA and shell model are shown in Fig. 3. They refer to the following two cases: (i) By neglecting the muon binding energy ϵ_b in Eq. (31) the elastic momentum transfer is the same for all nuclei, i.e. $q \approx m_\mu \approx 0.535 fm^{-1}$ (results denoted QRPA(i)). (ii) By taking into account ϵ_b in Eq. (31), the elastic momentum transfer is $q \approx m_\mu - \epsilon_b$ and varies from $q \approx 0.529 fm^{-1}$, for ^{48}Ti where $\epsilon_b \approx 1.3 MeV$, to $q \approx 0.482 fm^{-1}$, for ^{208}Pb where $\epsilon_b \approx 10.5 MeV$ (results indicated as QRPA(ii)). From the

variation of the coherent nuclear matrix elements M_{coh}^2 with respect to A and Z illustrated in Fig. 3(a) (photonic mechanism), and Fig. 3(b) (non-photonic mechanism), we see that by taking into consideration the muon binding energy ϵ_b , QRPA(ii), all matrix elements increase continuously up to the Pb region where they become about a factor of two larger than the approximate results of case (i). This implies that the coherent rate becomes larger for heavy nuclei, Pb region, which makes such nuclei attractive from an experimental point of view [6, 21] provided, of course, that they satisfy other additional criteria, as the minimization of the reaction background etc. [4, 5]. The (μ^-, e^-) conversion electrons of a given target are expected to show a pronounced peak around $E_e = m_\mu - \epsilon_b$ (for lead region $E_e \approx 95 MeV$).

The above results have been obtained using the factorization approximation Eq. (54). This approximation only slightly affects the ratio η of the coherent rate to the total rate. However, the branching ratio $R_{\mu e}$ for heavy nuclei is appreciably affected by using exact muon wave function. This gives results which for heavy nuclei are 30 – 40% larger than the approximate ones.

We should also note that, it is important to estimate the effect of the ground state RPA correlations on the (μ^-, e^-) matrix elements. This can be done by using a correlated quasi-particle RPA vacuum instead of the uncorrelated one. In Ref. [29] such calculations have been performed using the correlated vacuum defined by [46, 47]

$$|\tilde{0}\rangle = N_0 e^{\hat{S}^+} |0\rangle \quad (66)$$

where the operator \hat{S}^+ contains the correlation matrix and N_0 is an appropriate normalization factor. In this case, the coherent rate matrix elements take the form

$$\langle \tilde{0} | \hat{T} | \tilde{0} \rangle = N_0^2 \langle 0 | \hat{T} | 0 \rangle \quad (67)$$

which means that the correlated matrix elements are obtained by rescaling the uncorrelated ones (a similar expression holds for the total rate matrix elements). It was found that the matrix elements for ^{48}Ti obtained this way [29] are reduced by $\approx 30\%$ and that the ground state correlations tend to decrease the strengths of all (μ^-, e^-) conversion channels.

6.1.2 Incoherent process

The results for the incoherent rate obtained with “state-by-state” QRPA calculations of all the excited states for a series of nuclei throughout the periodic table are shown in Table 2 for the photonic diagrams, and Fig. 4 for the non-photonic ones. Positive and negative parity states up to 6^- , 6^+ are included. For the photonic mechanism only the vector component, S_V gives non-zero contribution ($M_{inc}^2 = S_V$). For the non-photonic mechanism we have non zero contributions from both the vector and axial vector components, S_V and S_A , ($M_{inc}^2 = S_V + 3S_A$).

It can be seen that, the main contribution to the incoherent rate comes from the 1^- multipolarity. For every multipole only the low-lying excited states give significant contributions. High-lying excited states contribute negligibly. Furthermore, the incoherent matrix elements do not show clear A and Z dependence. Their magnitude depends on the spectrum of the individual nuclear isotope.

In obtaining the results of Table 2 and Fig. 4 for 1^- states, the spurious center of mass contaminations, which arise from the use of empirical single particle energies and the truncation of the model space, have been eliminated by explicitly calculating the purely spurious state

$|S\rangle$ and removing its admixtures from the incoherent and total rates. The calculation of the overlaps $\langle 1^-, m|S\rangle$ (where m counts the 1^- contaminated excited states) have shown that mostly the spuriousity lies in the lowest 1^- state being $\sim 80\%$ for ^{48}Ti and ^{208}Pb (for other nuclei see Ref. [32]). We showed that in a good approximation we can neglect the first 1^- state, but then we have to renormalize the strengths of the residual interaction (Bonn potential). From the renormalization we found that the incoherent $\mu^- \rightarrow e^-$ conversion rate is not sensitive to the strength parameters of the two-body interaction, which increases the reliability of the RPA results. For all nuclei studied, the spurious center of mass contribution is less than 30% of the incoherent matrix elements, i.e., $\sim 2\%$ of the total (μ^-, e^-) conversion rate. Furthermore, even after removal of the spurious components the 1^- multipolarity appears to be the most important incoherent channel.

The explicit construction of all final nuclear states enables the calculation of the mean excitation energy \bar{E} needed in the closure approximation. Though \bar{E} is defined in analogy with the ordinary muon capture reaction by Eq. (65), the values of the “mean excitation energies” obtained in the (μ^-, e^-) are completely different than those evaluated in (μ^-, ν_μ) [29] because in the last process the coherent channel doesn’t exist. For the (μ^-, e^-) process the coherent channel appears only in the denominator of Eq. (65) and, since this dominates the total $\mu - e$ conversion rate, the resulting mean excitation energy \bar{E} in this process is much smaller than that for the (μ^-, ν_μ) reaction (see Table 3).

6.2 Comparison of coherent and incoherent processes

As we have seen in sect. 4, a useful quantity for the (μ^-, e^-) conversion is the fraction η of the coherent matrix elements M_{coh}^2 divided by the total one M_{tot}^2 . In earlier calculations η was estimated [7] to be a decreasing function of A with a value of $\eta \approx 83\%$ in Cu region. By using, however, local density approximation [28] and QRPA [31] we find that the coherent channel dominates throughout the periodic table.

The values of η obtained with QRPA are a bit larger than the more accurate results obtained with a local density approximation [28] (LDA) in the medium and heavy nuclei region. The reason is the following: The LDA, for the part of non-coherent contributions, uses neither closure nor explicit summation over all final states. It makes a summation over the continuum of excited states (even though they contribute negligibly they are infinite in number) in a local Fermi sea. The incoherent rate obtained this way, is tied to the number of states one can excite; the larger the better; the muon mass provides the energy for the excitation of such states. Consequently, LDA takes into account the contribution of the continuum spectrum and calculates it more accurately for heavier nuclei. Such contributions are absent from the RPA results for every nucleus.

6.3 Limits of the elementary sector part of $R_{\mu e^-}$. Calculation of $\gamma(A, Z)$

The task of studying the nuclear physics aspects of the exotic (μ^-, e^-) conversion process is to evaluate the function $\gamma(A, Z)$ of Eqs. (34), (37), (45) and (47). In general, the nuclear matrix elements entering $\gamma(A, Z)$ depend on the final nuclear state populated during process (3). The values for $\gamma(A, Z)$ calculated from the coherent QRPA matrix elements are shown in Table 4 and compared with the results of Refs. [27, 28]. The variation of $\gamma(A, Z)$ through the periodic table [27] exhibits a strong dependence on the neutron excess ($N - Z$) which mainly reflects the

dependence on (A, Z) of the total muon capture rate. We should note that, the muon binding energy ϵ_b of Eq. (31), which affects significantly the nuclear form factors for heavy nuclei like ^{208}Pb , affects also the factor $E_e p_e / m_\mu^2$ in the definition of γ Eq. (34). This factor takes into account the phase space in the transition matrix elements. By ignoring ϵ_b , this factor becomes unity. For ^{48}Ti this factor, by including ϵ_b , is equal to 0.97 and its neglect is a good approximation. For ^{208}Pb , however, this factor is equal to 0.81 which means that, in heavy nuclei the dependence on ϵ_b of the phase space cannot be ignored.

By putting the experimental limits [5, 6] of the branching ratio $R_{\mu e^-}$ on Eq. (33) we determine upper bounds on the parameter ρ for photonic, Z-exchange and W-box diagrams both in conventional extensions of the standard model as well as SUSY theories (for the currently interesting nuclei ^{48}Ti and ^{208}Pb see Table 4). We note that the values of ρ for ^{48}Ti are slightly improved over those of Table 2 of Ref. [29], but those of ^{208}Pb are appreciably smaller than those of sect. 5.1 of Ref. [27]. This big difference is due to the fact that, in the present work we have used the experimental limit of Ref. [6]. This experiment at PSI improved on the previous limit [21] of ^{208}Pb , which was used in Ref. [27], by an order of magnitude. For both nuclei we found that, the limits obtained from various nuclear models do not significantly differ from each other. We should stress, however, that, the different limits for ^{208}Pb in the shell model results of Table 4, are due to the neglect of ϵ_b in Eq. (31) when calculating the nuclear form factors as mentioned above; its consideration gives similar results to those of LDA and QRPA for both mechanisms. This implies that all nuclear models studied here give about same values for ρ .

One can use the limits of ρ to parametrize the muon number violating quantities entering Eqs. (38), (40), (46) and (48) and also to compare them directly to the value given from gauge models. As an example, we quote the value of $\rho = 8.2 \times 10^{-18}$ obtained in the supersymmetric model of Ref. [27] discussed above. This prediction of ρ is considerably smaller compared to the values listed in Table 4, which were extracted from experiment.

7 Summary and Conclusions

The main conclusions stemming out of the results discussed above can be summarized as follows. The coherent mode dominates throughout the periodic table indicated from the fact that $\eta \geq 90\%$.

The quasi-particle RPA and Local Density Approximation results for the (μ^-, e^-) rate do not show maximum around $A \approx 60$ as had previously estimated. This rate keeps increasing up to heaviest nuclei, i.e. region of ^{208}Pb , presently used at PSI as target. In evaluating the nuclear matrix elements the muon binding energy should not be ignored especially for heavy nuclei.

The great part of the incoherent rate comes from the low-lying excitations. The 1^- state gives the maximum incoherent contribution even after removing the spurious admixtures.

In contrast to the ordinary muon capture, the mean excitation energy, \bar{E} , of the nucleus in $\mu^- \rightarrow e^-$ is very small, $\bar{E} \approx 1\text{MeV}$.

The dependence of $R_{\mu e^-}$ on nuclear physics in coherent production, expressed by the function $\gamma(A, Z)$ shows a large variation. Thus, for example, in the case of photonic mechanism, γ lies in the region $1.6 \leq \gamma_{ph} \leq 26.0$ from lighter to heavier nuclei.

All nuclear models used give about the same values for γ and quantity ρ which contains the elementary sector parameters of the branching ratio $R_{\mu e^-}$. The quantity ρ is useful to fix the lepton flavour violating parameters and test the various gauge models.

The observation of any muon number (and in general any lepton and/or flavour number) non-conserving process, will reveal “new physics” beyond the standard model. The predicted branching ratios, however, are much smaller than experimental limits. The most optimistic results are obtained in the context of supersymmetry $1.2 \times 10^{-18} \leq R_{\mu e^-} \leq 2.4 \times 10^{-16}$

Although the predicted branching ratios for $\mu^- \rightarrow e^-$ process is much smaller than present-day experimental sensitivity, this should not discourage the relevant experiments, since it is a common belief that we do not as yet have a complete theory to adequately describe such exotic processes.

T.S.K. is grateful to the Organizing Committee of the Conference for financial support and the hospitality at Dubna.

References

- [1] R. Engfer and H.K. Walter, *Ann. Rev. Nucl. Part. Sci.* **36** (1986) 327.
- [2] J.D. Vergados, *Phys. Reports* **133** (1986) 1.
- [3] T.S. Kosmas, G.K. Leontaris and J.D. Vergados, *Prog. Part. Nucl. Phys.* **33** (1994) 397.
- [4] P. Depommier and C. Leroy, *Rep. Prog. Phys.* **58** (1995) 61.
- [5] H.K. Walter, in these proceedings, and Private communication.
- [6] W. Honecker *et al.*, (SINDRUM II Collaboration), *Phys. Rev. Lett.* **76** (1996) 200.
- [7] S. Weinberg and G. Feinberg, *Phys. Rev. Lett.* **3** (1959) 111; *ibid* E 244.
- [8] W.J. Marciano and A.I. Sanda, *Phys. Rev. Lett.* **38** (1977) 1512.
- [9] T.P. Cheng and L.F. Li, *Phys. Rev D* **20** (1979) 1608.
- [10] G. Altareli *et al.*, *Nucl. Phys. B* **125** (1977) 285.
- [11] O. Shanker, *Phys. Rev D* **20** (1979) 1608.
- [12] J. Bernabeu, E. Nardi and D. Tommasini, *Nucl. Phys. B* **409** (1993) 69.
- [13] T.S. Kosmas, G.K. Leontaris and J.D. Vergados, *Phys. Lett. B* **219** (1989) 457.
- [14] T.S. Kosmas and J.D. Vergados, *Phys. Reports* **264** (1996) 251.
- [15] J.D. Vergados and M. Ericson, *Nucl. Phys. B* **195** (1982) 262; S. Pittel and J.D. Vergados, *Phys. Rev. C* **24** (1981) 2343; G.K. Leontaris and J.D. Vergados, *Nucl. Phys. B* **224** (1983) 137; J.D. Vergados, *Phys. Rev. D* **23** (1981) 703.
- [16] J. Steinberger and H. Wolfe, *Phys. Rev* **110** (1955) 1490.

- [17] M. Conversi *et al.*, Phys. Rev **122** (1961) 687.
- [18] D.A. Bryman *et al.*, Phys. Rev **Lett.** **28** (1972) 1469.
- [19] A. Badertscher *et al.*, Nucl. Phys. **A 377** (1982) 406.
- [20] D.A. Bryman *et al.*, Phys. Rev. **Lett.** **55** (1985) 465.
- [21] S. Ahmad *et al.*, (TRIUMF Collaboration), Phys. Rev. **Lett.** **59** (1987) 970; Phys. Rev. **D 38** (1988) 2102.
- [22] A. Badertscher *et al.*, J. of Phys. **G 17** (1991) S47.
- [23] C. Dohmen *et al.*, (SINDRUM II Collaboration), Phys. Lett. **B 317** (1993) 631.
- [24] A. van der Schaaf, Nucl. Phys. **A 546** (1992) 421c; Prog. Part. Nucl. Phys. **31** (1993) 1.
- [25] T.S. Kosmas and J.D. Vergados, Phys. Lett. **B 215** (1988) 460.
- [26] T.S. Kosmas and J.D. Vergados, Phys. Lett. **B 217** (1989) 19.
- [27] T.S. Kosmas and J.D. Vergados, Nucl. Phys. **A 510** (1990) 641.
- [28] H.C. Chiang, E. Oset, T.S. Kosmas, A. Faessler and J.D. Vergados, Nucl. Phys. **A 559** (1993) 526.
- [29] T.S. Kosmas, J.D. Vergados, O. Civitarese and A. Faessler, Nucl. Phys. **A 570** (1994) 637.
- [30] T.S. Kosmas, A. Faessler and J.D. Vergados, J. of Phys. **G 23** (1997) 693.
- [31] T.S. Kosmas, A. Faessler, F. Šimkovic and J.D. Vergados, Phys. Rev. **C 56** (1997) 526.
- [32] J. Schwieger, A. Faessler, and T.S. Kosmas, Phys. Rev. **C 57**, in press.
- [33] F. Scheck, Phys. Reports **44** (1978) 187.
- [34] B. Goulard and H. Primakoff, Phys. Rev. **C 10** (1974) 2034;
D. Duplain, B. Goulard, and J. Joseph, Phys. Rev. **C 12** (1975) 28;
- [35] T. Suzuki, D. Mearsday and J. Roalsvig, Phys. Rev. **C 35** (1987) 236.
- [36] R.D. Bolton *et al.*, Phys. Rev. **D 38** (1988) 2077.
- [37] U. Bellgardt *et al.*, SINDRUM Collaboration, Nucl. Phys. **B 299** (1988) 1.
- [38] A. Bean *et al.*, Phys. Rev. **Lett.** **70** (1993) 138.
- [39] B.E. Matthias *et al.*, Phys. Rev. **Lett.** **66** (1991) 2716.
- [40] S. Kovalenko, in these proceedings.
- [41] T.S. Kosmas and J.D. Vergados, Phys. Rev. **D 55** (1997) 1752.
- [42] T.S. Kosmas *et al.*, in preparation.
- [43] T.S. Kosmas and J.D. Vergados, Nucl. Phys. **A 523** (1992) 72.

- [44] J. Heisenberg, R. Hofstadter, J.S. McCarthy and I. Sick, Phys. Rev. **Lett.** **23** (1969) 1402;
T.W. Donnelly and J.D. Walecka, Ann. Rev. Nucl. Sci. **25** (1975) 329;
B. Frois and C.N. Papanicolas, Ann. Rev. Nucl. Part. Sci. **37** (1987) 133.
- [45] H. de Vries, C.W. de Jager and C. de Vries, Atomic Data and Nuclear Data Tables **36** (1987) 495.
- [46] E.A. Sanderson, Phys. Lett. **19** (1965) 141;
J. Da Providencia, Phys. Lett. **21** (1966) 668.
- [47] D.J. Rowe, Nuclear collective motion, (Methuen and CO. LTD., London, 1970).

Table 1. Best upper limits for the branching ratios of some muon number violating processes: Elementary particle decay modes and exotic neutrinoless muon decays in a nucleus.

Process	Best upper limit	Reaction	Ref.
Elementary muon number violating processes			
$\mu \rightarrow e\gamma$	$R_{e\gamma} < 4.9 \times 10^{-11}$		[36]
$\mu \rightarrow ee^+e^-$ ($\mu \rightarrow 3e$)	$R_{3e} < 1.0 \times 10^{-12}$		[37]
$\tau \rightarrow \mu\gamma$	$R_\tau < 4.2 \times 10^{-6}$		[38]
$\tau \rightarrow \mu e^+e^-$,			
$\tau \rightarrow e\mu^+\mu^-$			
$\tau \rightarrow \mu\mu^+\mu^-$			
$(\mu^+e^-) \leftrightarrow (\mu^-e^+)$	$R_{M\bar{M}} < 6.5 \times 10^{-7}$		[39]
Neutrinoless rare muon decays in a Nucleus			
$\mu^-(A, Z) \rightarrow e^-(A, Z)^*$	$R_{\mu e^-} < 7.0 \times 10^{-13}$	$\mu^-Ti \rightarrow e^-Ti$	[5]
	$R_{\mu e^-} < 4.9 \times 10^{-11}$	$\mu^-Pb \rightarrow e^-Pb$	[6]
$\mu^-(A, Z) \rightarrow e^+(A, Z - 2)$	$R_{\mu e^+} < 5.5 \times 10^{-12}$	$\mu^-Ti \rightarrow e^+Ca$	[22]

TABLE 2. Incoherent $\mu - e$ conversion matrix elements (M_{inc}^2) for the photonic mechanism. Only the vector component (S_V) of the $\mu - e$ conversion operator (see Eq. (27)) contributes.

J^π	${}^{48}_{22}Ti$	${}^{60}_{28}Ni$	${}^{72}_{32}Ge$	${}^{112}_{48}Cd$	${}^{162}_{70}Yb$	${}^{208}_{82}Pb$
0^+	1.946	1.160	2.552	2.088	4.305	2.512
2^+	0.242	0.738	1.396	2.669	6.384	2.342
4^+	0.004	0.005	0.015	0.021	0.063	0.056
6^+	$6 \cdot 10^{-6}$	$6 \cdot 10^{-6}$	$1 \cdot 10^{-5}$	$6 \cdot 10^{-5}$	$2 \cdot 10^{-4}$	$3 \cdot 10^{-4}$
1^-	3.711	4.215	5.066	5.282	4.824	4.533
3^-	0.037	0.081	0.152	0.249	0.542	0.476
5^-	$2 \cdot 10^{-4}$	$2 \cdot 10^{-4}$	$5 \cdot 10^{-4}$	0.001	0.005	0.005
M_{inc}^2	5.940	6.199	9.181	10.309	16.123	9.924

Table 3. Mean excitation energies for some representative nuclei in the reaction: $\mu_b^- + (A, Z) \rightarrow e^- + (A, Z)^*$. In contrast to the ordinary muon capture reaction, where $\bar{E} \approx 20 \text{ MeV}$, in the $\mu - e$ conversion \bar{E} is very smaller.

Nucleus	^{48}Ti	^{60}Ni	^{72}Ge	^{112}Cd	^{162}Yb	^{208}Pb
\bar{E} (MeV)	0.84	0.44	0.50	0.40	0.44	0.28

Table 4. The new limits on the elementary sector part of the exotic $\mu - e$ conversion branching ratio extracted by using Eq. (33) and the recent experimental data for the nuclear targets ^{208}Pb , ^{48}Ti , [5, 6]. The nuclear part of the branching ratio, described by the function $\gamma(A, Z)$ (see sect. 4), is also shown.

		^{48}Ti		^{208}Pb	
Method	Mechanism	$\gamma(A, Z)$	$\rho (\times 10^{-13})$	$\gamma(A, Z)$	$\rho \times 10^{-12}$
QRPA	Photon exch.	9.42	≤ 4.6	17.33	≤ 2.7
	W-boson exch.	25.31	≤ 1.7	49.22	≤ 0.9
	SUSY s-lept.	25.61	≤ 1.7	49.50	≤ 0.9
	SUSY Z-exch.	110.57	≤ 0.4	236.19	≤ 0.2
LDA	Photonic	9.99	≤ 4.3	17.84	≤ 2.6
	W-boson exch.	26.60	≤ 1.6	55.53	≤ 0.8
SM	Photonic	9.74	≤ 4.4	10.42	≤ 4.4
	W-boson exch.	26.50	≤ 1.6	27.43	≤ 1.7

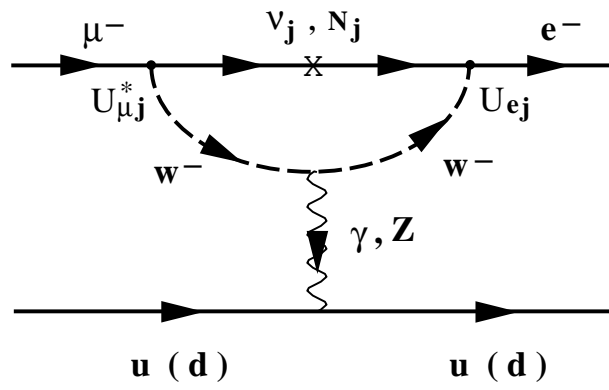
FIGURE CAPTIONS

FIGURE 1. Typical diagrams entering the neutrinoless (μ^-, e^-) conversion: photonic 1(a), Z-exchange 1(a),(b) and W-boson exchange 1(c), for the specific mechanism involving intermediate neutrinos.

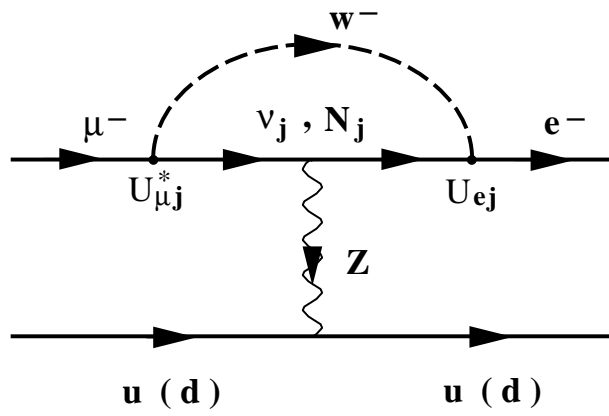
FIGURE 2. SUSY diagrams leading to the (μ^-, e^-) conversion: photonic 2(a), Z-exchange 2(a),(b) and box diagrams 2(c), in a supersymmetric model with charged s-lepton and neutralino mixing are shown. Note that, the Z-exchange in 2(b) as well as in Fig. 1(b), comes out of electrically neutral particles (photon exchange does not occur in these diagrams). These Z-exchange diagrams may be important (those of Figs. 1(a) and 2(a) are suppressed by m_μ^2/m_Z^2).

FIGURE 3. Variation of the coherent (μ^-, e^-) conversion matrix elements M_{coh}^2 for specific mass A and charge Z (see text) for the photonic mechanism (a) and the non-photonic mechanism (b). In QRPA(i) the muon binding energy ϵ_b was neglected, but it was included in QRPA(ii). We see that ϵ_b strongly affects the matrix elements for heavy nuclei. For comparison the results of Ref. [27] (shell model results) are also shown. For photonic and non-photonic diagrams the coherent rate increases up to *Pb* region where it starts to decrease.

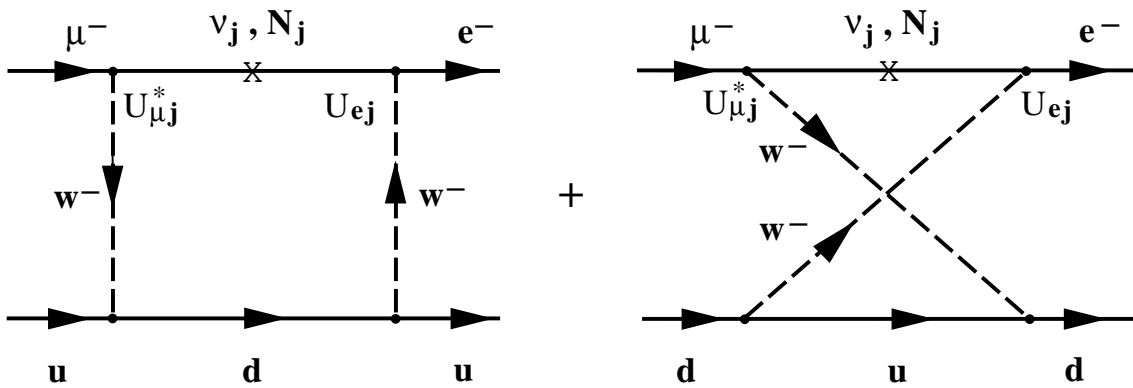
FIGURE 4. Incoherent non-photonic (μ^-, e^-) conversion rate for the most interesting nuclei from an experimental point of view; ^{208}Pb is currently used as a target in the SINDRUM II experiment at PSI and ^{48}Ti has provided the most stringent limit on the flavour violation. The bars show the partial contribution of each multipolarity of the $\mu \rightarrow e$ conversion operator (black bars for the vector part (S_V) and empty bars for the axial vector part (S_A)). The 1^- contribution shown is obtained after removing the spurious contaminations but still it is the most important one for this process.



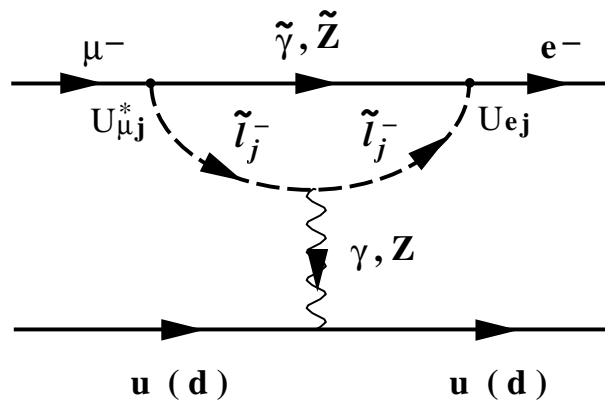
(a)



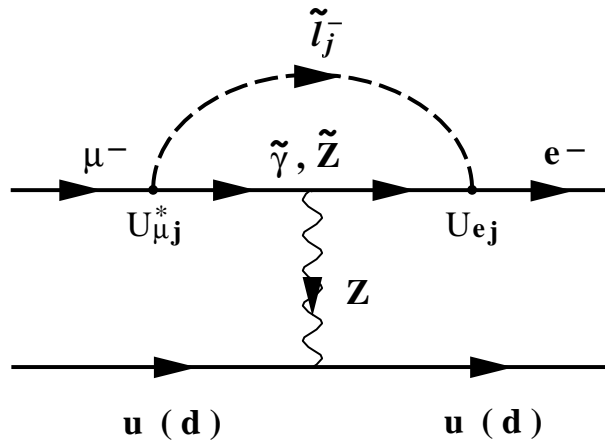
(b)



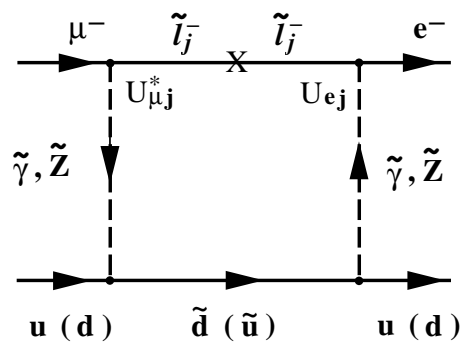
(c)



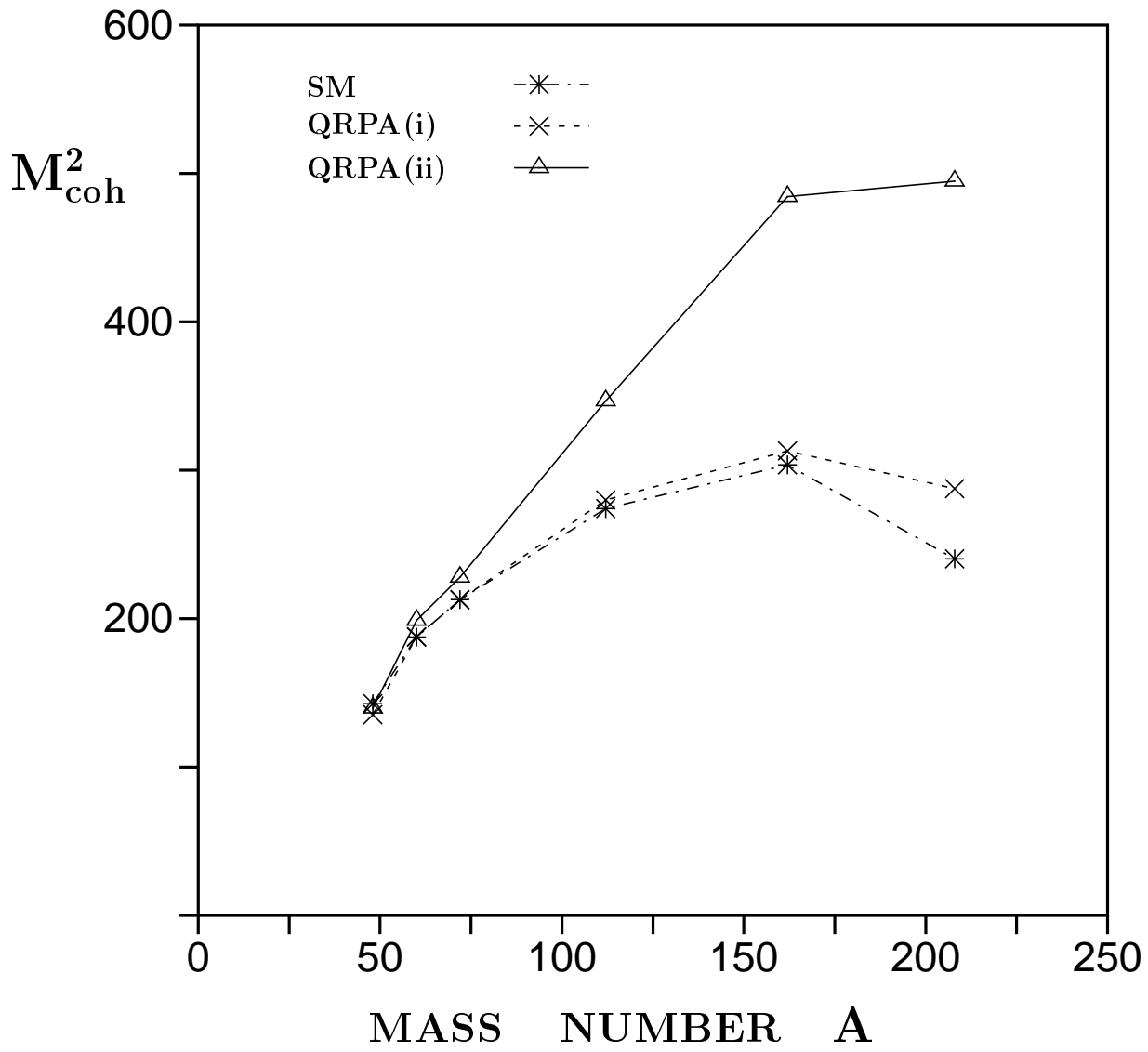
(a)



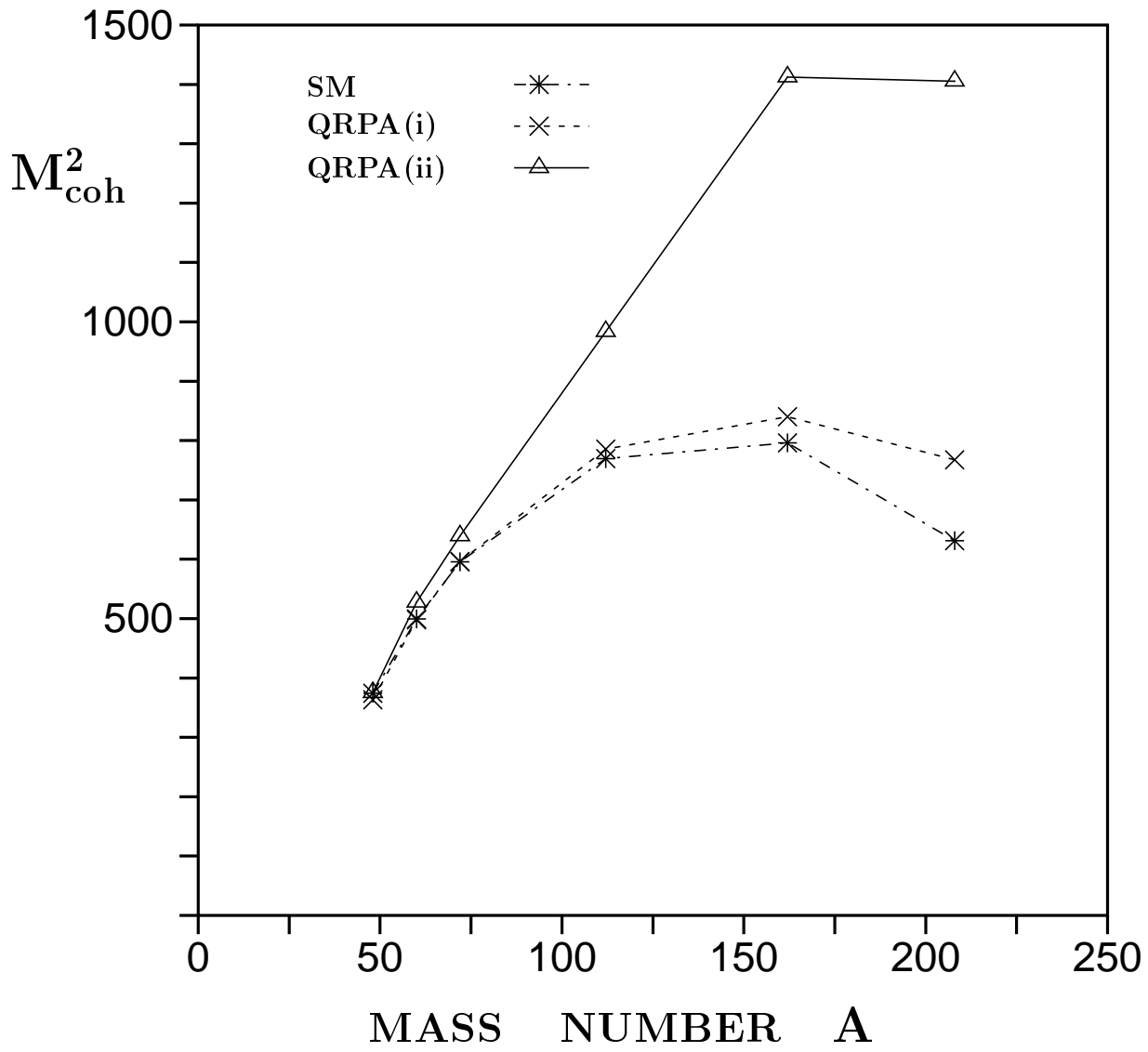
(b)



(c)



(a)



(b)

